



Development of a quantitative proteomics approach for cyclooxygenases and lipoxygenases in parallel to quantitative oxylipin analysis allowing the comprehensive investigation of the arachidonic acid cascade

Nicole M. Hartung¹ · Malwina Mainka¹ · Rebecca Pfaff¹ · Michael Kuhn¹ · Sebastian Biernacki¹ · Lilli Zinnert¹ · Nils Helge Schebb¹

Received: 18 July 2022 / Revised: 7 December 2022 / Accepted: 14 December 2022 / Published online: 23 January 2023
© The Author(s) 2023

Abstract

Oxylipins derived from the cyclooxygenase (COX) and lipoxygenase (LOX) pathways of the arachidonic acid (ARA) cascade are essential for the regulation of the inflammatory response and many other physiological functions. Comprehensive analytical methods comprised of oxylipin and protein abundance analysis are required to fully understand mechanisms leading to changes within these pathways. Here, we describe the development of a quantitative multi-omics approach combining liquid chromatography tandem mass spectrometry–based targeted oxylipin metabolomics and proteomics. As the first targeted proteomics method to cover these pathways, it enables the quantitative analysis of all human COX (COX-1 and COX-2) and relevant LOX pathway enzymes (5-LOX, 12-LOX, 15-LOX, 15-LOX-2, and FLAP) in parallel to the analysis of 239 oxylipins with our targeted oxylipin metabolomics method from a single sample. The detailed comparison between MRM³ and classical MRM-based detection in proteomics showed increased selectivity for MRM³, while MRM performed better in terms of sensitivity (LLOQ, 16–122 pM vs. 75–840 pM for the same peptides), linear range (up to 1.5–7.4 μ M vs. 4–368 nM), and multiplexing capacities. Thus, the MRM mode was more favorable for this pathway analysis. With this sensitive multi-omics approach, we comprehensively characterized oxylipin and protein patterns in the human monocytic cell line THP-1 and differently polarized primary macrophages. Finally, the quantification of changes in protein and oxylipin levels induced by lipopolysaccharide stimulation and pharmaceutical treatment demonstrates its usefulness to study molecular modes of action involved in the modulation of the ARA cascade.

Keywords Targeted proteomics · Targeted oxylipin metabolomics · Arachidonic acid cascade · Liquid chromatography tandem mass spectrometry · Multiple reaction monitoring cubed · Human macrophages

Abbreviations

aa	Amino acid	DFT	Dynamic fill time
ALOX5	Gene of the 5-lipoxygenase enzyme (5-LOX)	DP	Declustering potential
ARA	Arachidonic acid	EP	Entrance potential
CAD	Collisionally activated dissociation	FFT	Fixed fill time
CE	Collision energy	FLAP	Five-lipoxygenase-activating protein
COX	Cyclooxygenase	FWHM	Full width at half maximum
CSF	Colony-stimulating factors	GM-CSF	Granulocyte-macrophage colony-stimulating factor
CXP	Collision cell exit potential	HETE	Hydroxyeicosatetraenoic acid
		HHT	Hydroxyheptadecatrienoic acid
		IFN γ	Interferon γ
		IL-4	Interleukin 4
		IS	Internal standard
		LC	Liquid chromatography
		LIT	Linear ion trap

✉ Nils Helge Schebb
nils@schebb-web.de

¹ Chair of Food Chemistry, Faculty of Mathematics and Natural Sciences, University of Wuppertal, Gaußstr. 20, 42119 Wuppertal, Germany

LLOQ	Lower limit of quantification
LOD	Limit of detection
LOX	Lipoxygenase
LPS	Lipopolysaccharide
LT	Leukotriene
M-CSF	Macrophage colony-stimulating factor
MRM	Multiple reaction monitoring
MRM ³	Multiple reaction monitoring cubed
MS	Mass spectrometry
PBMC	Peripheral blood monocyctic cells
PBS	Phosphate buffered saline
PG	Prostaglandin
PTGS1/2	Genes of the prostaglandin G/H synthase 1/2 enzymes (COX-1 and COX-2)
P/S	Penicillin/streptomycin
TGF- β 1	Transforming growth factor- β 1
TRIS	Tris(hydroxymethyl)aminomethane
VD ₃	1,25-Dihydroxyvitamin D ₃

Introduction

The cyclooxygenase (COX) and lipoxygenase (LOX) pathways of the arachidonic acid (ARA) cascade play important roles in inflammation (simplified overview in Fig. 1). The formed eicosanoids and other oxylipins are potent lipid mediators of the immune response [1]. Through the initial oxidation of polyunsaturated fatty acids, such as ARA, via one of the two COX enzymes, the unstable prostaglandin (PG) H₂ is formed and can be further converted by downstream enzymatic or non-enzymatic reactions, e.g., to PGE₂ or 12-hydroxy-heptadecatrienoic acid (12-HHT) [2, 3]. Formed in immune cells, PGE₂ acts as a pro-inflammatory signaling molecule by, e.g., stimulating the upregulation of pro-inflammatory cytokines or enhancing blood flow through augmented atrial vasodilation [4, 5]. Increased PGE₂ levels are often associated with upregulated COX-2 (derived from the *PTGS2* gene) abundance that is induced by pro-inflammatory stimuli such as gram-negative bacteria [5]. Though biological functions of 12-HHT are not yet fully understood, recent studies have found this oxylipin to be involved i.a. in the mediation of allergic inflammation [6]. As chemical breakdown product of PGH₂, it is an established marker of COX activity [7]. The several LOX isoforms catalyze the stereo- and regiospecific formation of hydroperoxy fatty acids as primary products that are — in the cell — rapidly reduced to hydroxy fatty acids, e.g., hydroxyeicosatetraenoic acids (HETE) formed from ARA [8]. The LOX branch of the ARA cascade is also involved in inflammation regulation. 5-LOX catalyzes the formation of pro-inflammatory and chemotactic leukotrienes (LT), such as ARA-derived LTB₄. The multiple hydroxylated fatty acids

formed via consecutive LOX activity are believed to elicit anti-inflammatory properties involved in the active resolution of inflammation [8, 9] but remain controversially discussed [10]. The multitude of products arising from the many ARA cascade enzymes, crosstalk between the different branches, and various structurally distinct fatty acid substrates make a comprehensive oxylipin metabolomics platform necessary for thorough investigation of the oxylipin pattern. However, in order to fully comprehend the mechanisms leading to changes on metabolite levels, the additional investigation of gene expression, i.e., protein abundance, is indispensable.

In the recent years, interest in multi-omics techniques as tools to achieve systemic understanding of biological changes has drastically increased, i.e., metabolomics, proteomics, and transcriptomics [11, 12]. While liquid chromatography (LC) tandem mass spectrometry (MS/MS) is the standard method for quantitative targeted oxylipin analysis [13], the LC-MS/MS-based analysis of proteins has emerged in the recent years and is often conducted as high-throughput screenings allowing only relative quantification. Though the investigation of ARA cascade enzymes with proteomic tools has been reported [14–18], also in combination with metabolomics analyses [19, 20], a method for its quantitative analysis has not yet been described. Therefore, it was our goal to develop a targeted proteomics method comprising the important COX- and LOX-mediated signaling pathways and, together with our existing targeted oxylipin metabolomics platform [21–23], establishing a comprehensive and quantitative multi-omics tool to thoroughly investigate the ARA cascade.

Our targeted proteomics approach allows the analysis of human COX and LOX enzymes for the first time in a quantitative manner and, together with our oxylipin metabolomics method, is a valuable tool to characterize the ARA cascade from a single sample. This is demonstrated by characterizing the COX and LOX pathways in different human immune cells, showing correlations between oxylipin and protein abundances as well as quantitative changes upon pharmacological intervention.

Materials and methods

Chemicals and biological material

Fetal calf serum (superior standardized) was purchased from Biochrom (Berlin, Germany); 1,25-dihydroxyvitamin D₃ (VD₃) and ML351 as well as oxylipin standards were purchased from Cayman Chemical (Ann Arbor, MI, USA; local supplier Biomol, Hamburg, Germany). HEK293 cell-derived recombinant human transforming growth factor- β 1 (TGF- β 1), recombinant human colony-stimulating factors

Arachidonic Acid Cascade

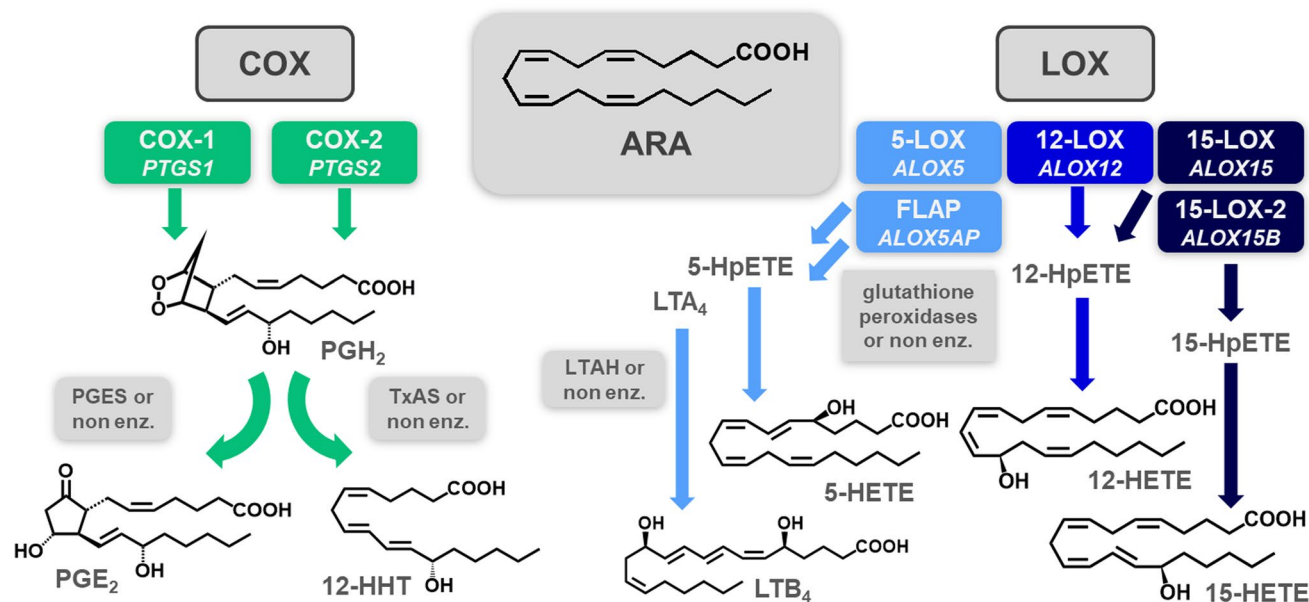


Fig. 1 Simplified overview of the cyclooxygenase (COX) and lipoxygenase (LOX) branches of the arachidonic acid (ARA) cascade. COX catalyzes the formation of prostaglandin (PG) H₂ which is further converted by downstream enzymes or non-enzymatically, e.g., to PGE₂ by PGE synthases (PGES) or to 12-hydroxy-heptadecatrienoic acid (12-HHT) by thromboxane A synthase (TxAS). The different LOX isoforms each oxidize ARA regioselectively to hydroperoxy-

eicosatetraenoic acids (HpETE) or leukotriene A₄ (LTA₄) in case of 5-LOX supported by the 5-LOX-activating protein (FLAP). The primary products are reduced to their respective hydroxy eicosatetraenoic acids (HETE) by, e.g., glutathione peroxidases or rapidly hydrolyzed to LTB₄ in case of LTA₄ (gene names are noted under the enzyme/protein in *italics*)

CSF-1 (M-CSF), CSF-2 (GM-CSF), interferon γ (IFN γ), and interleukin 4 (IL-4) produced in *Escherichia coli* were obtained from PeproTech Germany (Hamburg, Germany). Lymphocyte separation medium was purchased at PromoCell (Heidelberg, Germany). Human AB serum was provided by the blood donation center University Hospital Düsseldorf (Düsseldorf, Germany). Protease inhibitor mix M (AEBSE, Aprotinin, Bestatin, E-64, Leupeptin and Pepstatin A) and resazurin as well as MS approved trypsin ($> 6.000 \text{ U g}^{-1}$, from porcine pancreas) were from SERVA Electrophoresis GmbH (Heidelberg, Germany). Unlabeled AQUA peptide standards were obtained from Thermo Life Technologies GmbH (Darmstadt, Germany), unlabeled and heavy labeled (lys, uniformly labeled (U)- $^{13}\text{C}_6$; U- $^{15}\text{N}_2$; arg, U- $^{13}\text{C}_6$; U- $^{15}\text{N}_4$) peptide standards were purchased from JPT Peptides (Berlin, Germany).

Acetonitrile (HPLC–MS grade), acetone (HPLC grade), methanol, and acetic acid (both Optima LC–MS grade) were obtained from Fisher Scientific (Schwerte, Germany). Dithiothreitol was from AppliChem (Darmstadt, Germany). Tris(hydroxymethyl)aminomethane (TRIS), ammonium bicarbonate, sodium deoxycholate, and urea were obtained from Carl Roth (Karlsruhe, Germany). RPMI 1640, L-glutamine, and penicillin/streptomycin (5000 units penicillin

and 5 mg streptomycin mL^{-1}), lipopolysaccharide (LPS) from *E. coli* (0111:B4), dextran 500 from *Leuconostoc* spp., iodoacetamide, dimethylsulfoxide (DMSO), dexamethasone, indomethacin, celecoxib, and PF-4191834 as well as all other chemicals were purchased from Sigma (Schnellendorf, Germany).

Cell cultivation

THP-1 cells were obtained from the German Collection of Microorganisms and Cell Cultures GmbH (DSMZ, Braunschweig, Germany) and were maintained in bicarbonate buffered RPMI medium supplemented with 10% fetal calf serum, 100 U mL^{-1} penicillin, 100 $\mu\text{g mL}^{-1}$ streptomycin (P/S, 2%) and 2 mM L-glutamine (1%) in 60.1 cm^2 dishes in a humidified incubator at 37 °C and 5% CO₂. For experiments, cells were seeded at densities of $0.125 \cdot 10^6$ cells mL^{-1} and differentiated with 50 nM VD₃ (0.1% DMSO) and 1 ng mL^{-1} TGF- β 1 for 72 h.

Primary human macrophages were prepared as described by [24]. In brief, peripheral blood monocyctic cells (PBMC) were isolated from buffy coats obtained from blood donations at the University Hospital Düsseldorf. Blood samples were drawn with the informed consent of the human

subjects. The study was approved by the Ethical Committee of the University of Wuppertal. PBMC were isolated by dextran (5%) sedimentation for 45 min and subsequent centrifugation ($1000\times g$ without deceleration, 10 min, 20 °C) on lymphocyte separation medium. The leucocyte ring was isolated and washed twice with PBS. Cells were seeded in 60.1 cm² dishes and left to adhere for 1 h after resuspension in serum-free RPMI medium (2% P/S, 1% L-glutamine) in a humidified incubator at 37 °C and 5% CO₂ (8 dishes per donor). Cells were washed, and RPMI medium (2% P/S, 1% L-glutamine) supplemented with 5% human AB serum was added. For polarization towards M1- or M2-like macrophages, the medium was additionally supplemented with 10 ng mL⁻¹ CSF-2 or CSF-1 for 8 days and treated with 10 ng mL⁻¹ IFN γ or IL-4 for the final 48 h. No cytokines were added to generate M0-like macrophages.

Platelets were isolated from EDTA blood as described by the platelet-rich plasma method [25].

Cell culture experiments

For the experiments of the THP-1 cells or primary macrophages with test compounds, cell culture medium was replaced 7 h before the end of the differentiation with serum-free 50 mM TRIS-buffered RPMI medium (2% P/S, 1% L-glutamine) and the pharmacological inhibitors or DMSO (0.1%) as control were added. Cytotoxic effects of the test compounds at the used concentrations were excluded by resazurin (Alamar Blue) assay [26] and lactate dehydrogenase assay (ESM Figs. S4 and S5). After 1 h of preincubation, cells were additionally treated with 1 μ g mL⁻¹ LPS for 6 h. In case of the THP-1 cells, all adherent and non-adherent cells were harvested by scraping in the cell culture medium. Primary macrophages were harvested by cold shock method [24]. The harvested cell pellets were frozen at -80 °C until use.

Quantification of oxylipin and protein levels by LC-MS/MS

The presented methods allow the quantitative analysis of 239 oxylipins (ESM Table S4) and 11 proteins (Tables 1 and 2, ESM Table S7) from one cell pellet. Cells were resuspended in PBS containing 1% protease inhibitor mix and antioxidant solution (0.2 mg mL⁻¹ BHT, 100 μ M indomethacin, 100 μ M soluble epoxide hydrolase inhibitor *trans*-4-[4-(3-adamantan-1-yl-ureido)-cyclohexyloxy]-benzoic acid (*t*-AUCB) in MeOH [21, 22] and sonicated, and protein content was determined via bicinchoninic acid assay [27]. Internal standards (IS) for oxylipin analysis were added to the cell lysate before proteins were precipitated in methanol at -80 °C for at least 30 min. The supernatant after centrifugation ($20000\times g$, 10 min, 4 °C) served as sample for

oxylipin analysis, while the protein levels were later separately analyzed in the precipitated protein pellet after storage at -80 °C. For the oxylipin analysis, the supernatant after the protein precipitation was further purified according to the previously published method [21, 22] by solid-phase extraction on a non-polar (C8)/strong anion exchange mixed mode material (Bond Elut Certify II, 200 mg, Agilent, Waldbronn, Germany) and analyzed by LC-MS/MS. For the targeted LC-MS/MS-based proteomics analysis, the protein pellet obtained after the protein precipitation was resuspended in 5% (w/v) sodium deoxycholate containing 1% protease inhibitor mix and precipitated again in four volumes of ice-cold acetone after centrifugation ($15000\times g$, 20 min, 4 °C). Further steps were carried out as described by [18]. In brief, the dried protein pellet was re-dissolved in 6 M urea, the disulfide bridges were reduced with dithiothreitol, and the resulting free sulfhydryl groups were alkylated with iodoacetamide in order to inhibit the reformation of disulfide bridges. The samples were diluted with 50 mM NH₄HCO₃ before the tryptic digestion was carried out at a trypsin-to-protein ratio of 1:50. The digestion was stopped after 15 h by adding concentrated acetic acid to reduce the pH from \approx 7.8 to 3–4. A mixture of heavy labeled peptides (lys, U-¹³C₆; U-¹⁵N₂; arg, U-¹³C₆; U-¹⁵N₄) corresponding to each of the analytes was spiked as internal standards (final vial concentrations, 25 nM for COX and LOX peptides and 50/100 nM for the housekeeper peptides), before the samples were subjected to solid-phase extraction (Strata-X 33 μ m Polymeric Reversed Phase, Phenomenex LTD, Aschaffenburg, Germany) and analyzed by LC-MS/MS.

The samples for the oxylipin and peptide analysis were measured with separate methods on two 1290 Infinity II LC systems, each equipped with a Zorbax Eclipse Plus C18 reversed phase column (2.1 \times 150 mm, particle size 1.8 μ m, pore size 95 Å, Agilent) at 40 °C, with an upstream inline filter (3 μ m, 1290 infinity II inline filter, Agilent) and SecurityGuard Ultra C18 cartridge as precolumn (2.1 \times 2 mm). The oxylipins were separated as described by [21–23] with a gradient composed of 0.1% acetic acid mixed with 5% mobile phase B (mobile phase A) and acetonitrile/methanol/acetic acid (800/150/1, v/v/v; mobile phase B) at a flow rate of 0.3 mL min⁻¹: 21% B at 0 min, 21% B at 1.0 min, 26% B at 1.5 min, 51% B at 10 min, 66% B at 19 min, 98% B at 25.1 min, 98% B at 27.6 min, 21% B at 27.7 min, and 21% B at 31.5 min. The LC used for oxylipin analysis was coupled with a 5500 QTRAP mass spectrometer operated in negative electrospray ionization (ESI(-)) mode (Sciex, Darmstadt, Germany). The MS was set as follows: ion spray voltage, -4500 V; capillary temperature, 650 °C; curtain gas N₂, 50 psi; nebulizer gas (GS1) N₂, 30 psi; drying gas (GS2) N₂, 70 psi; generated with N₂ generator NGM 33 (cmc Instruments, Eschborn, Germany); and collisionally activated dissociation (CAD) gas, high. Declustering potentials (DP),

Table 1 MRM method parameters for (A) unlabeled and (B) heavy labeled (lys, U-¹³C₆; arg, U-¹⁵N₂; arg, U-¹³C₆; U-¹⁵N₂) peptides of COX-1, COX-2, 5-LOX, FLAP, 12-LOX, 15-LOX, and 15-LOX-2 used as internal standards (IS)

(A)													
Gene/protein (UniProtKB No.)	Peptide	Transitions	Q1 m/z	Q3 m/z	RT [min]	Rel. ratio to quantifier [%]	CE (V)	IS transitions	Calibration range [nM]	LOD [pM]	LLOQ [pM]	LOD peptide on column [fg]	LOD enzyme on column [pg]
PTGS1/cyclooxygenase-1 (COX-1; P23219)	DCPTPMGTK	M ²⁺ → y ₇ ⁺	503.7	731.4			19						
		M ²⁺ → b ₂ ⁺	503.7	276.1	6.92 ± 0.01	59	20	M ²⁺ → y ₇ ⁺	0.016–1570	7.9	16	37	2.7
		M ²⁺ → y ₅ ⁺	503.7	533.3		43	31						
		M ³⁺ → y ₅ ⁺	639.3	652.3			26						
		M ³⁺ → y ₄ ⁺	639.3	505.3	16.06 ± 0.03	57	28	M ³⁺ → y ₅ ⁺	0.50–5000	250	500	2394	86
PTGS2/cyclooxygenase-2 (COX-2; P35354)	AEHPTWGD-EQLFQTR	M ³⁺ → y ₆ ⁺	639.3	765.4		55	28						
		M ²⁺ → y ₇ ⁺⁺	561.8	430.7			25						
		M ²⁺ → y ₇ ⁺	561.8	860.4	20.44 ± 0.02	36	25	M ²⁺ → y ₇ ⁺⁺	0.021–2111	4.2	21	24	1.5
		M ²⁺ → b ₂ ⁺	561.8	263.1		25	24						
		M ²⁺ → y ₈ ⁺	627.8	956.3			29						
	NAIMSYVLTSR	M ²⁺ → b ₃ ⁺	627.8	299.1	17.81 ± 0.02	86	27	M ²⁺ → y ₈ ⁺	0.25–5000	100	250	627	34
		M ²⁺ → y ₉ ⁺	627.8	1069.6		43	27						
		M ²⁺ → y ₇ ⁺	500.3	773.3			23						
		M ²⁺ → b ₂ ⁺	500.3	227.2	18.03 ± 0.02	62	22	M ²⁺ → y ₇ ⁺	0.027–2660	13	27	66	4.6
		M ²⁺ → y ₅ ⁺	500.3	547.3		30	25						
ALOX5/5-lipoxygenase (5-LOX; P09917)	DDGLLVWEAIR	M ²⁺ → y ₆ ⁺	643.8	773.4			30						
		M ²⁺ → y ₇ ⁺	643.8	886.5	23.38 ± 0.01	81	28	M ²⁺ → y ₆ ⁺	0.122–1219	49	122	313	19
		M ²⁺ → y ₅ ⁺	643.8	674.4		85	25						
		M ²⁺ → y ₇ ⁺	657.4	773.5			28						
		M ²⁺ → y ₁₀ ⁺	657.4	1086.6	22.12 ± 0.01	66	30	M ²⁺ → y ₆ ⁺	0.25–5000	100	250	656	39
ALOX5AP/arachidonate 5-lipoxygenase-activating protein (FLAP; P20292)	TGTLAFER	M ²⁺ → y ₈ ⁺	657.4	886.5		43	30						
		M ²⁺ → y ₅ ⁺	447.7	635.4			22						
		M ²⁺ → y ₃ ⁺	447.7	451.2	11.30 ± 0.02	70	24	M ²⁺ → y ₄ ⁺	0.074–7366	37	74	165	3.4
		M ²⁺ → y ₆ ⁺	447.7	736.4		55	20						
		M ²⁺ → y ₇ ⁺	552.3	793.4			24						
ALOX12/12-lipoxygenase (12-LOX; P18054)	LWEIAR	M ²⁺ → b ₂ ⁺	552.3	311.1	16.27 ± 0.03	67	24	M ²⁺ → y ₇ ⁺	0.010–5000	5.0	10	28	0.45
		M ²⁺ → y ₆ ⁺	552.3	694.4		69	26						
		M ²⁺ → y ₅ ⁺	450.8	601.4			21						
		M ²⁺ → b ₂ ⁺	450.8	300.2	18.51 ± 0.02	32	17	M ²⁺ → y ₆ ⁺	0.025–5000	10	25	45	3.8
		M ²⁺ → y ₆ ⁺	450.8	787.4		21	21						
AVLNQFR	AVLNQFR	M ²⁺ → y ₅ ⁺	424.2	677.4			19						
		M ²⁺ → y ₄ ⁺	424.2	564.3	11.07 ± 0.02	47	21	M ²⁺ → y ₅ ⁺	0.050–5000	25	50	106	9.5
		M ²⁺ → y ₃ ⁺	424.2	450.3		6	19						

Table 1 (continued)

(A)	ALOX15/15-lipoxygenase (15-LOX; P16050)	EITEIGLQ- GAQDR	M ²⁺ → y ₈ ⁺	715.4	844.4					34							
			M ²⁺ → y ₅ ⁺	715.4	546.3	13.62 ± 0.01	38			32						402	21
			M ²⁺ → y ₉ ⁺	715.4	957.5		29			35							
	GFPVSLQAR		M ²⁺ → y ₇ ⁺⁺	487.8	385.7					20							
			M ²⁺ → y ₅ ⁺	487.8	574.3	14.78 ± 0.01	28			29						250	37
			M ²⁺ → y ₇ ⁺	487.8	770.5		18			24						487	
	ALOX15B/15-lipoxygenase-2 (15-LOX-2; O15296)	ELLIVPGQVVD	M ²⁺ → y ₇ ⁺	669.4	770.4					30							
			M ²⁺ → b ₅ ⁺	669.4	568.4	18.76 ± 0.02	32			24						147	8.3
			M ²⁺ → y ₈ ⁺	669.4	869.5		32			29							
	VSTGEAFGAGT-WDK		M ²⁺ → y ₇ ⁺	713.3	734.3					36							
			M ²⁺ → y ₈ ⁺	713.3	881.4	14.42 ± 0.02	83			36						250	38
			M ²⁺ → y ₉ ⁺	713.3	952.5		79			35							
(B)	Geno/protein (UniProtKB No.)	Peptide	Transitions	Q1 m/z	Q3 m/z	RT [min]	Rel. ratio to quantifier [%]	CE (V)									
	PTGS1/cyclooxygenase-1 (COX-1; P23219)	DCPTPMGK	M ²⁺ → y ₇ ⁺	507.7	739.4			19									
			M ²⁺ → b ₂ ⁺	507.7	276.1	6.92 ± 0.01	59			20							
			M ²⁺ → y ₇ ⁺⁺	507.7	370.2		17			23							
	AEHPTWGD-EQLFQTTR		M ³⁺ → y ₅ ⁺	642.6	662.4			26									
			M ³⁺ → y ₄ ⁺	642.6	515.3	16.06 ± 0.03	53			28							
			M ³⁺ → y ₆ ⁺	642.6	775.4		50			28							
	PTGS2/cyclooxygenase-2 (COX-2; P35354)	FDPELLFNK	M ²⁺ → y ₇ ⁺⁺	565.8	434.8			25									
			M ²⁺ → y ₇ ⁺	565.8	868.5	20.44 ± 0.02	34			25							
			M ²⁺ → y ₄ ⁺	565.8	529.3		6			33							
	NAIMSYVLTSR		M ²⁺ → y ₈ ⁺	632.8	966.3			29									
			M ²⁺ → b ₃ ⁺	632.8	299.2	17.81 ± 0.02	92			27							
			M ²⁺ → y ₇ ⁺	632.8	835.5		70			30							
	PTGS1/COX-1 & PTGS2/COX-2	LILIGETIK	M ²⁺ → y ₇ ⁺	504.3	781.5			23									
			M ²⁺ → y ₆ ⁺	504.3	668.4	18.03 ± 0.02	23			24							
			M ²⁺ → y ₈ ⁺	504.3	894.6		4			24							
	ALOX5/5-lipoxygenase (5-LOX; P09917)	DDGLLVWEAIR	M ²⁺ → y ₆ ⁺	648.8	783.4			30									
			M ²⁺ → y ₇ ⁺	648.8	896.5	23.38 ± 0.01	78			28							
			M ²⁺ → y ₅ ⁺	648.8	684.4		83			25							
	NLEAIVSIAER		M ²⁺ → y ₆ ⁺	662.4	684.4			28									
			M ²⁺ → y ₈ ⁺	662.4	896.5	22.12 ± 0.01	76			30							
			M ²⁺ → y ₄ ⁺	662.4	498.3		36			28							

Table 1 (continued)

ALOX5AP/ arachidonate 5-lipoxygenase- activating protein FLAP; P20292	TGTLAFER	M ²⁺ → y ₄ ⁺	452.7	532.2			24
		M ²⁺ → y ₅ ⁺	452.7	645.4	11.30 ± 0.02	44	22
		M ²⁺ → y ₃ ⁺	452.7	461.2		32	24
	YFVGYLGER	M ²⁺ → y ₇ ⁺	557.3	803.4			24
ALOX12/12- lipoxygenase (12-LOX; P18054)		M ²⁺ → b ₂ ⁺	557.3	311.1	16.27 ± 0.03	66	24
		M ²⁺ → y ₆ ⁺	557.3	704.4		72	26
	LWEIAR	M ²⁺ → y ₆ ⁺	455.8	797.5			21
		M ²⁺ → y ₄ ⁺	455.8	482.3	18.51 ± 0.02	87	21
AVLNQFR		M ²⁺ → y ₃ ⁺	455.8	369.2		44	21
		M ²⁺ → y ₅ ⁺	429.2	687.4			19
		M ²⁺ → y ₃ ⁺	429.2	460.3	11.07 ± 0.02	7	19
		M ²⁺ → z ₄ ⁺	429.2	557.3		6	28
ALOX15/15- lipoxygenase (15-LOX; P16050)	EITEIGLQ- GAQDR	M ²⁺ → y ₈ ⁺	720.4	854.4			34
		M ²⁺ → y ₅ ⁺	720.4	556.3	13.62 ± 0.01	39	32
		M ²⁺ → y ₉ ⁺	720.4	967.5		30	35
	GFPVSLQAR	M ²⁺ → y ₇ ⁺⁺	492.8	390.7			20
ALOX15B/15- lipoxygenase-2 (15-LOX-2; O15296)		M ²⁺ → y ₅ ⁺	492.8	584.3	14.78 ± 0.01	28	29
		M ²⁺ → y ₆ ⁺	492.8	683.4		10	30
	ELLIVPGVVDR	M ²⁺ → y ₇ ⁺	674.4	780.4			30
		M ²⁺ → y ₈ ⁺	674.4	879.5	18.76 ± 0.02	30	29
VSTGEAFGAGT- WDK		M ²⁺ → b ₅ ⁺	674.4	568.4		30	24
		M ²⁺ → y ₇ ⁺	717.3	742.4			36
		M ²⁺ → y ₈ ⁺	717.3	889.4	14.42 ± 0.02	74	36
		M ²⁺ → y ₁₂ ⁺⁺	717.3	624.3		58	30

For each peptide, different collisionally activated dissociation fragment ions used for qualification and quantification (top) with their Q1 and Q3 *m/z* are shown with retention time (RT), mean ± SD, set of *n* = 23 calibrators) and relative ratios to quantifier transition as well as collision energies (CE). For unlabeled peptides (A), the linear calibration range is shown for quantifier transitions as well as the transitions of the corresponding heavy labeled peptides used as internal standards (IS) for quantification, limits of detection (LOD), lower limits of quantification (LLOQ), and LOD of the peptides and enzymes on column. Accuracy of calibrators was within a range of ± 15% (20% for LLOQ). The concentrations of all heavy labeled peptides (IS) in the vial are 25 nM

Table 2 MRM³ method parameters for (A) unlabeled and (B) heavy labeled (lys, U-¹³C₆; U-¹⁵N₂; arg U-¹³C₆; U-¹⁵N₄) peptides of COX-1, COX-2, 5-LOX, FLAP, 12-LOX, 15-LOX, and 15-LOX-2 used as internal standards (IS)

(A)

Protein	Peptide	Mode	Transition (Q1 → Q3)	Q1 <i>m/z</i>	Q3 <i>m/z</i>	<i>m/z</i> of MS ³ fragment ions summed for MRM ³	Time period [min]	RT [min]	CE (V)	AF2 (V)	Calibra- tion range [nM]	LOD [nM]	LLOQ [nM]	LOD pep- tide on column [pg]	LOD enzyme on column [pg]
PP1B COX-1	IGDEDVGR	MRM	*	*	*	-	0.00–6.61	5.99 ± 0.01	*	-	*	-	-	-	-
	DCPTPMGTK	MS ³	M ²⁺ → y ₇ ⁺	503.7	731.4	713.4 (b ₇ ⁺), 644.3, 695.3, 533.3 (y ₅ ⁺), 515.3 (y ₅ ⁺ — H ₂ O), 567.4, 585.3 (b ₆ ⁺), 608.3, 677.3, 387.2	6.61–9.10	6.92 ± 0.01	19	0.08	0.079–31	0.031	0.079	0.15	11
FLAP	TGTLAER	MS ³	M ²⁺ → y ₅ ⁺	447.7	635.4	617.3 (b ₅ ⁺), 416.2, 277.2, 287.3, 600.4, 382.2, 434.3, 522.3 (y ₄ ⁺), 461.2 (b ₄ ⁺), 332.2 (b ₃ ⁺)	9.10–12.45	11.30 ± 0.01	24	0.08	1.5–368	1.1	1.5	4.9	100
	EITEIGLQ- GAQDR	MS ³	M ³⁺ → y ₅ ⁺	477.2	546.3	528.3 (b ₅ ⁺), 511.2, 330.1, 384.1, 401.2, 215.2, 244.1, 290.1 (y ₂ ⁺), 372.2 (b ₄ ⁺), 418.2 (y ₃ ⁺)	12.45–14.40	13.63 ± 0.01	21	0.07	0.84–113	0.56	0.84	4.0	211
CYC1 GAPDH	DVCTFLR	MRM	*	*	*	-	14.40–17.03	14.85 ± 0.03	*	-	*	-	-	-	-
	GALQNIIPAST- GAAK	MRM	*	*	*	-	14.40–17.03	15.09 ± 0.03	*	-	*	-	-	-	-
β-γ-actin	VAPEHPV- LLTEAPLNPK	MRM	*	*	*	-	14.40–17.03	15.68 ± 0.04	*	-	*	-	-	-	-
	LILGETIK	MS ³	M ²⁺ → y ₇ ⁺	500.3	773.3	755.5 (b ₇ ⁺), 609.4, 496.3, 361.2 (y ₃ ⁺), 310.3, 547.3, (y ₅ ⁺), 383.3, 451.3, 514.3 (b ₅ ⁺), 591.4	17.03–18.26	18.03 ± 0.01	23	0.12	0.13–4.0	0.053	0.13	0.27	18
12-LOX	LWEIAR	MS ³	M ²⁺ → y ₅ ⁺	450.8	601.4	583.4 (b ₅ ⁺), 472.3 (y ₄ ⁺), 338.3, 342.2, 229.3, 310.3, 359.2 (y ₃ ⁺), 356.2 (b ₃ ⁺), 243.1 (b ₂ ⁺), 409.4	18.26–18.62	18.51 ± 0.01	21	0.07	0.075–25	0.050	0.075	0.23	19

Table 2 (continued)

15-LOX-2	ELLIVPGQV-VDR	MS ³	M ²⁺ → y ₇ ⁺	669.4	770.4	752.4 (b ₇ ⁺), 283.1 (b ₃ ⁺), 596.4 (b ₆ ⁺), 382.2 (b ₄ ⁺), 464.4, 436.6, 365.4, 337.2 (y ₆ ⁺⁺), 481.3 (b ₅ ⁺), 587.5	18.62–19.59	18.76 ± 0.01	30	0.13	0.44–22	0.22	0.44	1.5	83
COX-2	FDPELLFNK	MS ³	M ²⁺ → y ₇ ⁺⁺	561.8	430.7	634.4 (y ₅ ⁺), 227.1 (b ₂ ⁺), 521.3 (y ₄ ⁺), 340.2 (b ₃ ⁺), 408.2 (y ₃ ⁺), 763.4 (y ₆ ⁺), 261.2 (y ₂ ⁺), 745.3, 697.2, 373.2	19.59–21.90	20.44 ± 0.01	25	0.05	0.084–42	0.042	0.084	0.24	15
5-LOX	DDGLLVWEIAR	MS ³	M ²⁺ → y ₅ ⁺	643.8	674.4	359.2 (y ₃ ⁺), 387.2 (b ₃ ⁺), 316.1 (b ₂ ⁺), 656.4 (b ₆ ⁺), 324.5, 638.4, 612.4, 595.4, 344.4, 510.4	21.90–36.00	23.38 ± 0.01	25	0.11	0.49–122	0.37	0.49	2.4	144
(B)															
Protein	Peptide	Mode	Transition (Q1 → Q3)	Q1 m/z	Q3 m/z	m/z of MS³ fragment ions summed for MRM³	Time period [min]	RT [min]	CE (V)	AF2 (V)	IS concen- tration in vial [nM]				
PPIB	IGDEDVGR	MRM	*	*	*	-	0.00–6.61	5.99 ± 0.01	*	-	50				
COX-1	DCPTPMGTK	MS ³	M ²⁺ → y ₇ ⁺	507.7	739.4	652.3, 721.4 (b ₇ ⁺), 703.3, 387.2, 541.3 (y ₅ ⁺)	6.61–9.10	6.92 ± 0.01	19	0.08	25				
FLAP	TGTLAFER	MS ³	M ²⁺ → y ₅ ⁺	452.7	645.4	627.3 (b ₅ ⁺), 425.2, 277.2, 287.3, 391.2	9.10–12.45	11.30 ± 0.01	24	0.08	25				
15-LOX	EITEIGLQ- GAQDR	MS ³	M ³⁺ → y ₅ ⁺	480.6	556.3	538.3 (b ₅ ⁺), 372.2 (b ₄ ⁺), 521.2, 330.1, 226.1	12.45–14.40	13.63 ± 0.01	21	0.07	25				
CYC1	DVCTFLR	MRM	*	*	*	-	14.40–17.03	14.85 ± 0.03	*	-	50				
GAPDH	GALQNIIPAST- GAAK	MRM	*	*	*	-	14.40–17.03	15.09 ± 0.03	*	-	50				
β-γ-actin	VAPEHPV- LLEAPLNPK	MRM	*	*	*	-	14.40–17.03	15.68 ± 0.04	*	-	100				

Table 2 (continued)

COX-1/2	LILGETIK	MS ³	M ²⁺ → Y ₇ ⁺	504.3	781.5	496.3, 451.1, 310.2, 763.5 (b ₇ ⁺), 555.3 (Y ₅ ⁺)	17.03–18.26	18.03 ± 0.01	23	0.12	25
12-LOX	LWEIIR	MS ³	M ²⁺ → Y ₅ ⁺	455.8	611.3	593.4 (b ₅ ⁺), 482.3 (Y ₄ ⁺), 338.3, 351.2, 238.2	18.26–18.62	18.51 ± 0.01	21	0.07	25
15-LOX-2	ELLIVPGQV- VDR	MS ³	M ²⁺ → Y ₇ ⁺	674.4	780.4	283.1 (b ₃ ⁺), 762.4 (b ₇ ⁺), 382.2 (b ₄ ⁺), 365.4, 337.2	18.62–19.59	18.76 ± 0.01	30	0.13	25
COX-2	FDPELLFNK	MS ³	M ²⁺ → Y ₇ ⁺⁺	565.8	434.8	642.4 (Y ₅ ⁺), 227.1 (b ₂ ⁺), 771.4 (Y ₆ ⁺), 529.3 (Y ₄ ⁺), 340.2 (b ₃ ⁺)	19.59–21.90	20.44 ± 0.01	25	0.05	25
5-LOX	DDGLLWEIAR	MS ³	M ²⁺ → Y ₅ ⁺	648.8	684.4	369.2 (Y ₃ ⁺), 387.2 (b ₃ ⁺), 648.5, 352, 466.2	21.90–36.00	23.38 ± 0.01	25	0.11	25

The unlabeled and corresponding heavy labeled peptides from one protein were measured together in one time period covering each retention time (RT). RT are shown as mean ± SD, set of *n* = 19 calibrators. Shown are Q1 *m/z* and collisionally activated dissociation fragments (Q3) as well as selected MS³ fragments together with their respective collision (CE) and excitation energies (AF2). The linear trap (LIT) excitation time was set to 25 ms (standard setting) with fixed fill times of 250 ms (maximum) for all peptides (TGTLAFER = 100 ms, IS peptides, 25 ms) at a scan rate of 10 000 Da/s. The MS³ fragments were isolated from the MS³ spectra with an isolation window of ± 0.5 Da. The ratio between the sum of (A) 10 MS³ fragments of the unlabeled peptide and (B) 5 MS³ fragments of the heavy labeled peptide is used for quantification. The concentrations of the IS are shown in (B). The linear calibration range and the limits of detection (LOD), lower limits of quantification (LLOQ), and LOD of the peptides and enzymes on column are shown for (A) unlabeled peptides. The accuracy of the calibrators was within a range of ± 15% (± 20% for LLOQ). Additionally, peptides of four housekeeping proteins (GAPDH, PPIB, β-γ-actin, CYC1) were measured in MRM mode as separate periods with set dwell times of 20 ms and the parameters specified in ESM Table S7

* details are specified in ESM Table S7

entrance potentials (EP), collision cell exit potentials (CXP), and collision energies (CE) were optimized for each of the oxylipins. MS parameters for oxylipin analysis can be found in ESM Table S14 together with a detailed description of the standard series preparation (ESM Sect. 1). The oxylipin concentrations were quantified using external calibrations with IS, and they were normalized to the absolute protein content determined with bicinchoninic acid assay [27].

The peptides were chromatographically separated with a gradient composed of 95/5% water/acetonitrile (mobile phase A) and 5/95% water/acetonitrile (mobile phase B), both containing 0.1% acetic acid at a flow rate of 0.3 mL min⁻¹ as follows: 0% B at 0 min, 0% B at 1 min, 35% B at 30.5 min, 100% B at 30.6 min, 100% B at 33.5 min, 0% B at 33.7 min, and 0% B at 36 min. The LC system for peptide analysis was coupled to a 6500+ hybrid triple quadrupole linear ion trap mass spectrometer (QTRAP; Sciex) in ESI(+)-mode, with the following settings: ion spray voltage, 5500 V; capillary temperature, 550 °C; curtain gas N₂, 50 psi; nebulizer gas (GS1) N₂, 60 psi; and drying gas (GS2) N₂, 60 psi, generated with N₂ generator Eco Inert-ESP (DTW, Bottrop, Germany). DP, EP, and CXP were set to 40 V, 10 V, and 10 V, respectively, and CE were optimized for each of the peptides (Tables 1 and 2; ESM Table S7). CAD gas was set to medium. Analyst (Sciex, version 1.7) was used for instrument control and data acquisition, and Multiquant (Sciex, version 3.0.2) software was used for data analysis. The peptide/protein concentrations were quantified using external calibrations with IS (ESM Sect. 2.1; ESM Table S5; Tables 1 and 2; and ESM Table S7), and they were normalized to the absolute protein content determined with bicinchoninic acid assay [27].

Results

The ARA cascade plays a key role in the regulation of many different physiological processes. In order to understand the crosstalk between the different enzymatic pathways of the ARA cascade (Fig. 1) and modulation thereof, quantitative information for both oxylipin levels as well as enzyme/protein abundance is needed.

For this reason, we developed an analytical approach allowing to quantify the enzymes of the ARA cascade and combined it with our targeted oxylipin metabolomics method [21–23]. Combining targeted LC–MS/MS-based proteomics and oxylipin metabolomics as multi-omics methodology allows to quantify the abundance of all relevant enzymes of the COX and the LOX pathways (COX-1 and COX-2, 5-LOX, 12-LOX, 15-LOX, 15-LOX-2, and FLAP) as well as four housekeeping proteins and oxylipin levels from a single sample down to pM ranges.

Oxylipins were extracted from the methanolic supernatant resulting after sonication and precipitation of the cell samples, and enzyme/protein levels were quantified in the precipitated protein residue. Thus, only a *single* sample is required for quantitatively assessing the ARA cascade on metabolite and protein abundance levels in biological samples.

Targeted proteomics LC–MS/MS/(MS) method

The enzyme abundance is measured in form of representative peptides with amino acid (aa) sequences specific to the target enzyme. Based on an *in silico* tryptic digestion of the COX and LOX enzymes, two proteotypic peptides with unique [28, 29] aa sequences were selected per enzyme from the multitude of theoretically possible peptides (ESM Table S6). The results from the *in silico* digestion were narrowed down by a defined set of criteria [18] including fixed peptide lengths (7–22 aa) as well as acceptable calculated cleavage probabilities [30] (e.g., ≥ 70% using cleavage prediction with decision trees [31]) and predicted retention times (3–30 min) [32]. Possible variations in relevant splice variants [33] were considered as well as the presence of maximum two unfavored aa (C, M, N, Q, W). Peptides containing single nucleotide polymorphisms [33] or post-translational modifications were excluded [33, 34]. After the *in silico* peptide selection and evaluation of three to five candidates in digested cell matrix, the MS/MS parameters were optimized, and two peptides per protein were finally selected based on their MS sensitivity, selectivity, and chromatographic behavior (Tables 1 and 2; ESM Table S7).

In MS³ mode, the triple quadrupole QTRAP instrument uses the linear ion trap (LIT) in Q3 for a second fragmentation of the CAD fragment ions. With the aim of achieving higher selectivity and, thus, sensitivity for quantification of the peptides in complex biological matrices by this additional fragmentation, we chose an MS³ approach for the targeted proteomics method. For each peptide, the CE of multiple CAD fragment ions was optimized, and two to three of the most intense fragment ions, ideally with *m/z* exceeding the precursor ion *m/z* (e.g., a transition from a double charge precursor to a single charged fragment), were chosen for further evaluation in MS³ mode. Their excitation energies (AF2) were optimized in 0.01 V steps, and the final CAD fragment ions for the MS³ method were selected based on the highest sensitivities and/or lack of matrix interference in digested cell lysates for each peptide (Table 2).

The fixed fill time (FFT) for the LIT had a major impact on the signal intensity which increased with longer FFTs (ESM Fig. S1A). The maximum FFT of 250 ms provided the highest sensitivities and was thus used for all peptides (except abundant TGTLAER, 100 ms, and IS peptides,

25 ms). In order to allow the simultaneous analysis of all peptides with acceptable cycle times and, thus, data points per peak, the analytical run was split into 10 periods (i.e., time windows) with separate MS experiments. Despite excellent chromatographic separation (Table 2; Fig. 2A (i)), with average peak widths at half maximum height (FWHM) of 4.9 s, the number of initially selected peptides needed to be reduced to one peptide per protein for the MRM³ method. The selection was made based on the peptides' sensitivities and retention times to assure that all proteins are detected in the separate time windows of the chromatogram. At a LIT scan rate of 10000 Da s⁻¹, a total cycle time of 372–572 ms for each of the eight MS³ experiments resulted and thus 9–12 data points over the FWHM of the peak. The peptides of four housekeeping proteins were measured in two periods set in MRM mode with resulting cycle times of 150 and 450 ms at constant dwell times of 20 ms.

For data evaluation, MRM³ transitions were constructed from the MS³ spectra by the Multiquant 3.0.2 software. Assessing the MRM³ transitions of one MS³ fragment ion compared to the sum of multiple MS³ fragment ions showed higher signal intensity for the use of multiple fragment ions (ESM Fig. S2). Thus, for the final method, the ten most abundant MS³ fragment ions of the analyte peptides and five of the IS peptides were selected for data analysis.

The MS³ approach was compared to scheduled MRM detection. Here, the windows were set to ± 45 s at the expected retention time and a cycle time of 0.4 s resulting in comparable average 14 data points over FWHM of the chromatographic peaks. Two peptides per protein were included in the method comprising again all COX and relevant LOX pathway enzymes as well as four housekeeping proteins, resulting in a total of 23 peptides (Fig. 2A (ii), Table 1, ESM Table S7). The parallel measurement of three transitions per peptide ensures its identity by calculating the area ratios between one quantifier and two qualifier transitions and comparing the area ratios of the samples to the standards. As acceptance criteria, the ratios for a peak in a biological sample need to be within $\pm 20\%$ of the area ratio measured in standards (ESM Table S8) [18].

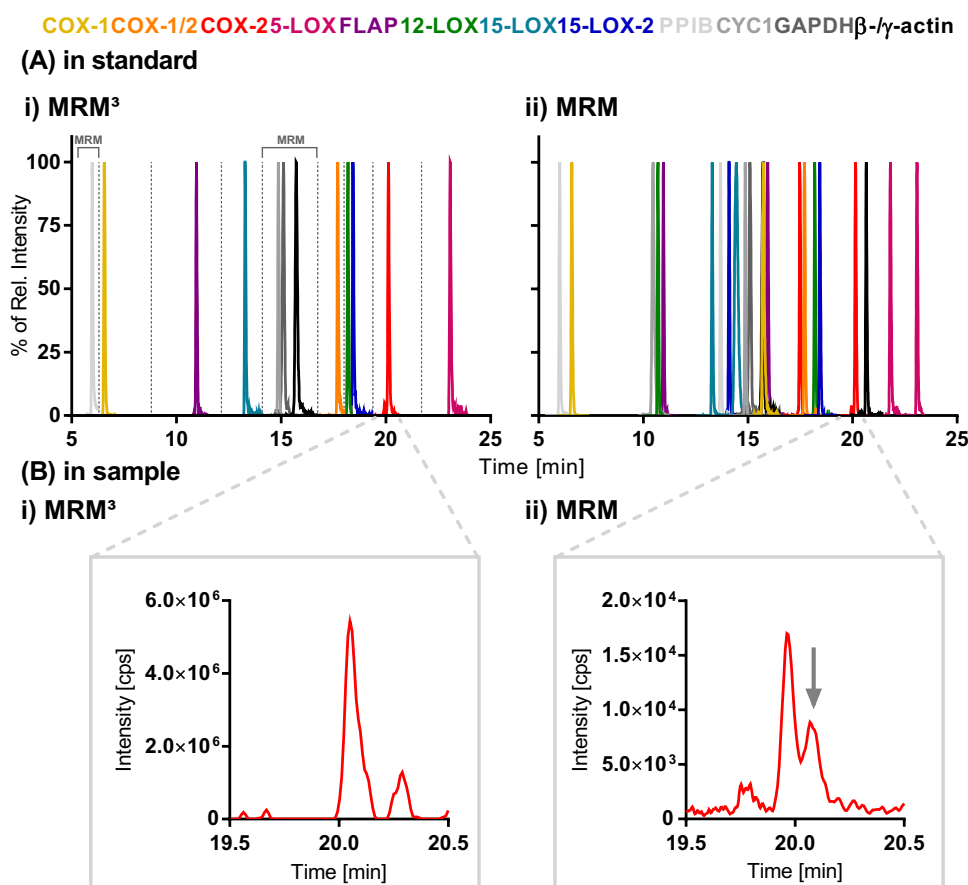
The additional fragmentation in MS³ increased selectivity allowing separation of the analyte from interfering matrix signals. This is shown in Fig. 2B (i) and (ii) for the low abundant COX-2 peptide FDPELLFNK in differentiated (50 nM VD₃ and 1 ng mL⁻¹ TGF- β 1, 72 h) and LPS-stimulated (1 μ g mL⁻¹, 6 h) THP-1 cells. The MRM³ method enables sensitive detection and quantification of COX and LOX peptides in the medium to high pM range (31–560 pM) (ESM Fig. S3; Table 2). However, the MRM method was more sensitive with up to tenfold lower limits of detection (LOD) ranging from 4.2 to 56 pM and lower limits of quantification (LLOQ) in the range of 16–122 pM for the same peptides (ESM Fig. S3; Table 1).

Overfilling of the trap at higher concentrations results in a breakdown of the MS signal (ESM Fig. S1B) and restricts the calibration range of the MRM³ method to 4.0–368 nM depending on the peptide (Table 2). This limits the linear working range of the MRM³ method to only two to three orders of magnitude. Here, the MRM method also shows a clear advantage allowing linear calibration over approximately five orders of magnitude from the pM LLOQ up to the low μ M range (Table 1). Thus, MRM is generally advantageous. If the analyte signal is interfered in matrix, MRM³ provides an additional level of selectivity and is useful for complicated biological matrices, while MRM is more sensitive and allows analysis within a large linear range. The developed method is not only sensitive but shows good precision and accuracy as demonstrated for the repeated independent analysis of THP-1 macrophages. The intraday precision was generally $\leq 15\%$, and interday precision was $< 30\%$ in the LPS-stimulated cells (ESM Table S9). The accuracy, determined after spiking the unstimulated cells with peptides during sample preparation, was between 95 and 140% (ESM Table S10). The dual approach of targeted oxylipin metabolomics and proteomics allows the analysis of oxylipin concentrations and protein levels in *one* sample. This powerful tool was applied to comprehensively analyze the ARA cascade in immune cells.

Analysis of the ARA cascade in immune cells

The lipid mediators formed in the ARA cascade are an essential part of the immune system and function i.a. as signaling molecules between different types of immune cells in the host defense. Using the developed LC-MS/MS-based proteomics platform together with the targeted oxylipin metabolomics method, the ARA cascade was comprehensively analyzed in human macrophages for the first time with this novel approach. The monocytes from the THP-1 cell line were examined during differentiation to macrophage-like cells with 50 nM VD₃ and 1 ng mL⁻¹ TGF- β 1 for 72 h. This process induced the *ALOX5* gene expression along with 5-LOX product formation (5-HETE and LTB₄) (Fig. 3A (i), (ii)). While other LOX were not present, COX-1 and FLAP levels increased by 17- and 32-fold, respectively, after differentiation. Additional treatment of the macrophages with 1 μ g mL⁻¹ LPS for 6 h stimulated *PTGS2* gene expression and formation of PGE₂ and 12-HHT which was below the detection limit in THP-1 cells bearing COX-1 alone (THP-1 monocytes and macrophages) (Fig. 3A (i), (ii)). The COX-2 protein level increased strongly after LPS (1 μ g mL⁻¹) treatment from below the detection limit (t_0) to approximately 80 fmol mg⁻¹ protein at the peak after 6–8 h where it declined to 40 fmol mg⁻¹ protein after 24 h (Fig. 3A (iii)). Pretreatment of the THP-1 macrophages with

Fig. 2 Chromatographic separation of the peptides from the COX and LOX enzyme pathways as well as housekeeping peptides with detection in (i) MRM³ and (ii) MRM mode on an LC–MS/MS QTRAP system. Shown are **A** (i) and (ii) a mix of peptide standards (25–100 nM) as well as **B** (i) and (ii) the signal of COX-2 peptide FDPELLFNK in THP-1 cells (i) MS³: M²⁺ → y₇⁺⁺ → Σ10 MS³ fragments; (ii) MRM: M²⁺ → y₇⁺⁺. The cells were differentiated for 72 h with vitamin D₃ (50 nM) and TGF-β1 (1 ng mL⁻¹) and treated with LPS (1 μg mL⁻¹) for 6 h



dexamethasone suppressed the induction of COX-2 and concomitant prostanoid synthesis with potencies (IC₅₀) of 3.4 nM (COX-2; 95% CI, 2.3–4.9 nM) and 1.2 nM (PGE₂; 95% CI, 0.9–1.6 nM), respectively (Fig. 3A (iv)). The 5-LOX inhibitor PF4191834 suppressed 5-HETE formation with a potency (IC₅₀) of 26 nM (95% CI, 12–53 nM) and did not affect the 5-LOX abundance (Fig. 3A (v)).

In the next step, we investigated the expression of ARA cascade genes and oxylipin formation in differently polarized primary human macrophages. The different types of polarization led to distinct oxylipin and protein patterns (Fig. 3B (i), (ii)). In M0-like macrophages, which were derived from primary monocytic cells and incubated without cytokines for 8 days, only COX-1 and 12-LOX as well as its product 12-HETE were detected. However, the presence of both enzymes is most likely attributed to platelet contamination which can be detected with our method since they are highly abundant in these cells (ESM Table S11). Relevant amounts of COX-1, 5-LOX, and FLAP (0.4 ± 0.1, 0.4 ± 0.2, and 19 ± 6 pmol mg⁻¹ protein, respectively) were found in the macrophages polarized towards M1-like cells (10 ng mL⁻¹ CSF-2 and 10 ng mL⁻¹ IFNγ) with the targeted proteomics method. Oxylipins formed via these pathways (PGE₂, 12-HHT, and 5-HETE) as well as 12- and 15-HETE were detected at low levels (≤ 5 pmol mg⁻¹

protein) in the cells (Fig. 3B (i), (ii); ESM Table S12). Stimulation with 1 μg mL⁻¹ LPS led to strong elevation of oxylipin concentrations, e.g., fourfold increase of PGE₂ and 12-HHT as well as an approximately tenfold increase of 5- and 15-HETE. *PTGS2* gene expression was induced by LPS, while the protein levels of COX-1 and FLAP were not modulated, and 5-LOX was slightly reduced. LC–MS analysis of the M2-like macrophages showed an extensive protein pattern: COX-1, 5-LOX, and FLAP as well as 15-LOX and 15-LOX-2 were present. High levels of 15-HETE (243 ± 20 pmol mg⁻¹ protein) as well as moderate levels of 12-HETE (21 ± 2 pmol mg⁻¹) and 12-HHT (19 ± 6 pmol mg⁻¹ protein) dominated the oxylipin profile, while PGE₂ and 5-HETE were found at approximately 2 pmol mg⁻¹ protein (Fig. 3B (i), (ii); ESM Table S12). Interestingly, the additional LPS treatment only led to an approximately twofold increase of PGE₂ and 12-HHT concentrations but did not affect any of the oxylipins from the LOX pathways. Apart from COX-2 induction, the levels of the ARA cascade enzymes were not changed by LPS (Fig. 3B (i), (ii)). While the COX-2 levels were similar in both (LPS-stimulated) M1- and M2-like cells, 5-LOX and FLAP levels were two- and fivefold higher in M1-like and COX-1 levels were higher in M2-like macrophages. However, all of the analyzed oxylipins were higher concentrated in M2-like

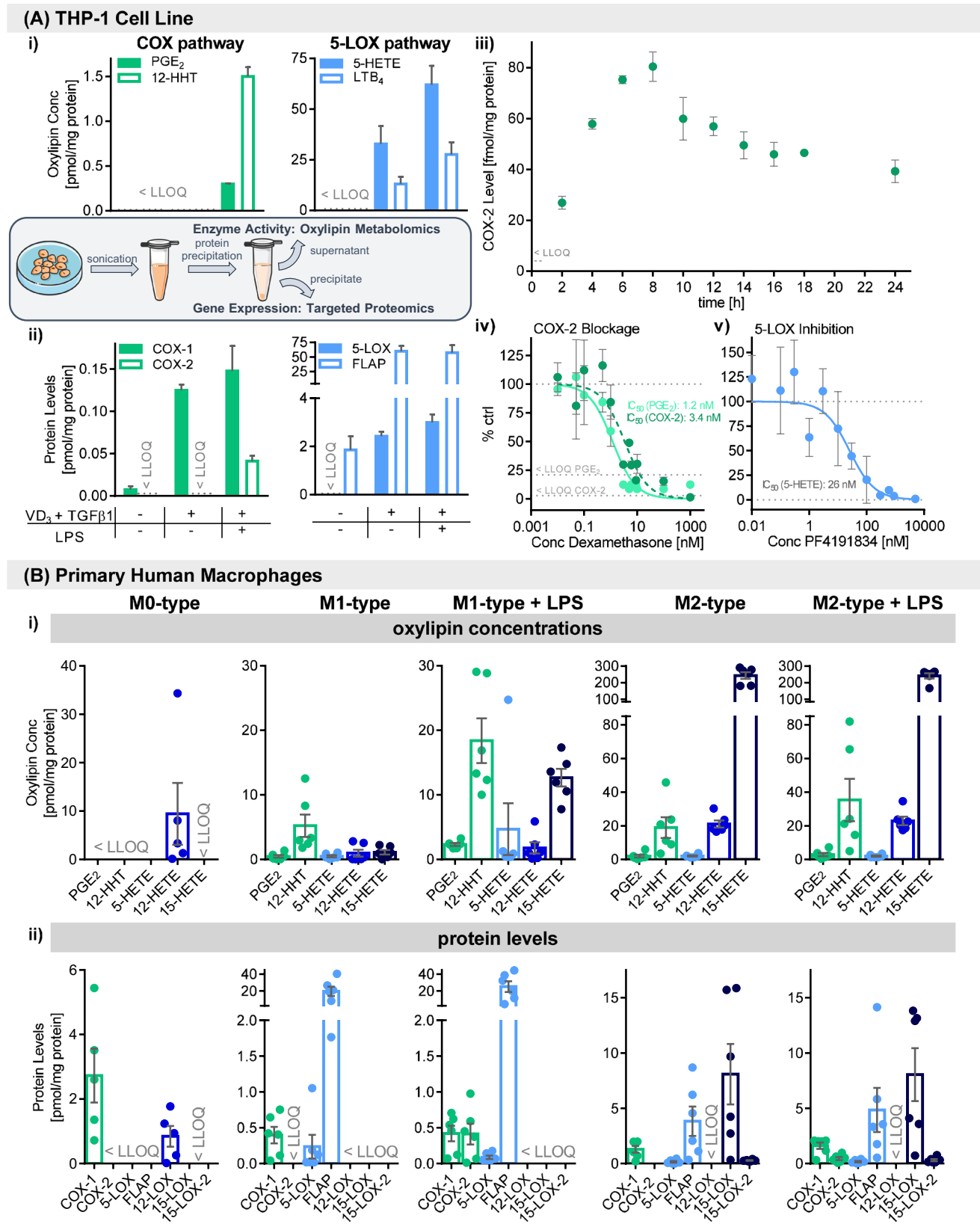


Fig. 3 Comprehensive characterization of immune cells using combined targeted oxylipin metabolomics and proteomics: **A** THP-1 cell line and **B** primary human macrophages. **A** (i) Oxylipin concentrations and (ii) enzyme levels in monocytic and macrophage-like THP-1 cell line with and without lipopolysaccharide (LPS) stimulation. Cells were differentiated to macrophages with 50 nM 1,25-dihydroxyvitamin D₃ (VD₃) and 1 ng mL⁻¹ TGF-β1 for 72 h, with or without LPS stimulation (1 μg mL⁻¹) for 6 h (mean ± SD, *n* = 3). **A** (iii) COX-2 abundance following time-dependent LPS stimulation (1 μg mL⁻¹). Shown are mean ± SD, *n* = 3. The potencies (IC₅₀) of COX-2 and 5-LOX inhibition by **A** (iv) dexamethasone, calculated based on PGE₂ formation and COX-2 abundance, and **A** (v) 5-LOX inhibitor PF4191834, calculated based on 5-HETE formation, relative to control incubations (0.1% DMSO). Shown are mean ± SD, *n* = 3 – 6. Correlation of **B** (i) oxylipin formation and (ii) enzyme levels in human macrophages derived from primary blood monocytic cells. Cells were differentiated with 10 ng mL⁻¹ CSF-2 (M1-like cells) or CSF-1 (M2-like cells) for 8 days. For the final 48 h, they were treated with 10 ng mL⁻¹ IFNγ (M1-like cells) or IL-4 (M2-like cells) and with or without 1 μg mL⁻¹ LPS for the final 6 h. For M0-like cells, the adhered monocytes were left untreated for 7 days. Shown are mean ± SEM, *n* = 5 – 6

macrophages with the most pronounced differences between M1- and M2-like cells found for 15-HETE (> 200-fold) and 12-HETE (approximately 20-fold) followed by PGE₂, 12-HHT, and 5-HETE (all approximately fourfold). Regarding the housekeeping proteins, only GAPDH showed strong differences between the M1- and M2-like macrophages indicating that it is not suited for normalization when investigating macrophage polarization (ESM Table S12).

The ARA cascade is an important target of pharmaceuticals because of its pivotal role in the regulation of the immune response and inflammation. We applied the multi-omics LC–MS/MS-based approach on the quantitative characterization of pharmaceutical modulation of the ARA cascade to demonstrate its usefulness in drug development (Fig. 4A, B; ESM Table S13).

For the experiments, the primary human macrophages polarized towards M1- or M2-like phenotype were pre-incubated with the test compounds at sub-cytotoxic levels (ESM Figs. S4 and S5) for 1 h before LPS was added for the remaining 6 h. The COX-1/COX-2 inhibitor indomethacin strongly reduced the PGE₂ and 12-HHT concentrations in both M1- and M2-like macrophages without relevantly modulating the COX-1 or COX-2 levels. Dexamethasone treatment also led to lowered concentrations of PGE₂ and 12-HHT with a more pronounced effect in M1 (approximately 50% inhibition) compared to M2-like cells (approximately 20% inhibition). The decrease of prostanoid concentrations occurred together with a decrease of the COX-2 levels which was similar in both types (approximately 40% inhibition) and did not affect COX-1. Both indomethacin and dexamethasone also markedly reduced 15-HETE formation in M1-like macrophages but had no effect in the M2-like cells. The celecoxib treatment of M2-like macrophages led to a moderate inhibition of the PGE₂ and 12-HHT formation,

while the concentrations of LOX products slightly increased. COX-2 and 15-LOX-2 levels were slightly reduced, and the selective COX-2 inhibitor did not affect COX-1 (Fig. 4A, B; ESM Table S13). The 5-LOX inhibitor PF4191834 hardly reduced the 5-HETE concentration in the M1-like macrophages. The PGE₂ and 12-HHT concentrations were unaffected by PF4191834, while the 12- and 15-HETE concentrations were slightly reduced. Regarding the 15-LOX pathway, ML351 led to a marked inhibition of both 12- and 15-HETE formation without affecting 15-LOX and 15-LOX-2 levels. 5-LOX abundance was strongly reduced (23 ± 4% of control) with only a slight effect on the 5-HETE concentration. In these incubations, the PGE₂ and 12-HHT concentrations were moderately increased, and the COX-1 and COX-2 levels were slightly elevated (Fig. 4A, B; ESM Table S13).

Conclusively, we combined our existing targeted oxylipin metabolomics method with an LC–MS/MS-based targeted proteomics method comprising all COX and relevant LOX pathway enzymes as well as four housekeeping proteins. While the more selective detection can be achieved with the MRM³ detection method, the MRM approach is characterized by higher sensitivity (in low pM range) and greater linear range up to μM concentrations. With our sensitive multi-omics approach, we were able to determine the oxylipin and protein levels of immune cells in a single sample. We successfully used this approach to thoroughly characterize the ARA cascade in different immune cells and demonstrated that quantitative changes induced by pharmaceutical modulation can be determined on protein and metabolite levels.

Discussion

Oxylipins formed in the ARA cascade act as potent lipid mediators regulating many physiological functions. In order to profoundly evaluate and understand modulation of this important signaling pathway, it is crucial to investigate not only changes in metabolite concentrations, i.e., eicosanoids and oxylipins, but also on enzyme levels in parallel. Therefore, we combined our targeted oxylipin metabolomics method covering 239 analytes (ESM Table S4) — allowing the quantitative characterization of the complex crosstalk between the different branches of the ARA cascade — with a novel LC–MS/MS-based targeted proteomics approach. The developed targeted proteomics method allows the quantitative analysis of all COX (COX-1 and COX-2) as well as relevant enzymes of the LOX pathway (5-LOX, 12-LOX, 15-LOX, 15-LOX-2, and FLAP) and four housekeeping proteins (β-/γ-actin, PPIB, GAPDH, CYC1). This is the first LC–MS/MS(/MS)-based method for the targeted analysis of the COX and LOX pathways of the ARA cascade.

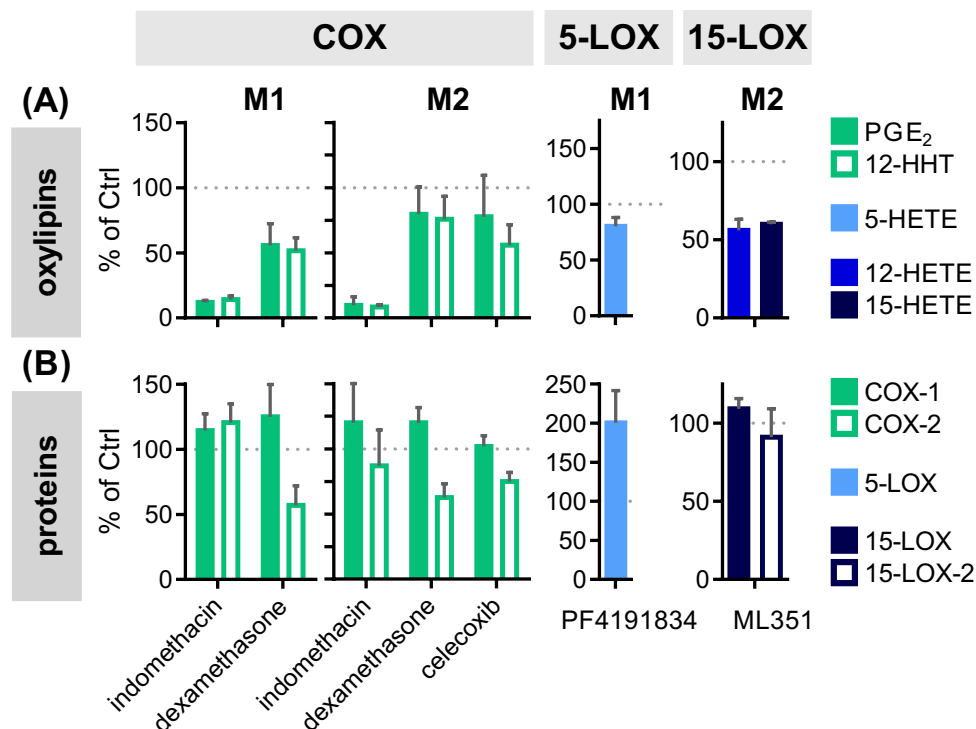


Fig. 4 Investigation of ARA cascade modulation in human macrophages using LC–MS/MS-based targeted **A** oxylipin metabolomics and **B** proteomics. Primary blood monocytic cells were differentiated to macrophages with 10 ng mL⁻¹ CSF-2 (M1-like cells) or CSF-1 (M2-like cells) for 8 days and with 10 ng mL⁻¹ IFN γ (M1-like cells) or IL-4 (M2-like cells) for the final 48 h. The cells were incubated with the different drugs at the following concentrations for the final

7 h during additional LPS stimulation (1 μ g mL⁻¹) for the final 6 h, 1 μ M COX-1/2 inhibitor indomethacin, 100 nM dexamethasone, 5 μ M COX-2 inhibitor celecoxib, 5 μ M 5-LOX inhibitor PF4191834, 10 μ M 15-LOX inhibitor ML351, or 0.1% DMSO as vehicle control. Relative product formation was calculated based on the mean of 2 controls per donor. Shown are mean \pm SEM, n = 3–5 donors

In targeted proteomics, different MS modes can be used for detection on hybrid triple quadrupole-LIT mass spectrometers. In MRM mode, the analytes are quantified via the pair of a precursor and a specific fragment ion resulting from CAD-based fragmentation. In MRM³, these CAD ions are again fragmented in the LIT, and an ion chromatogram is reconstructed from the secondary fragment ions [35]. We compared both approaches in detail. The LIT fill time had a strong effect on sensitivity of the MRM³ mode. FFT was preferred over dynamic fill time (DFT) due to its better signal reproducibility and accuracy based on the resulting identical cycle times for every sample [36]. The signal intensity increased with longer FFT (ESM Fig. S1A) in line with literature [36, 37]. Long FFTs, however, have the drawback of a more rapid exhaustion of LIT capacity and breakdown of the MS signal (ESM Fig. S1B). This generally limited the upper calibration range of our MRM³ method to low (4 nM) or medium (368 nM) nM concentrations (corresponding to 0.28–9.5 μ g mL⁻¹ enzyme equivalent) (Table 2), comparable to other proteomics applications of MRM³ where linearity was reported for concentrations up to 0.5–20 μ g mL⁻¹ [35, 36, 38]. Using MRM, however, robust quantification is

possible over a concentration range of five orders of magnitude up to low μ M concentrations (Table 1; ESM Table S7).

Summing the ten most abundant fragment ions from the MS³ spectra as “MRM³” during data evaluation enhanced sensitivity (ESM Fig. S2). In MRM³, the LODs of the COX and LOX peptides were in the low to medium pM range (equivalent to 11–209 pg enzyme on column) and the LLOQs ranged from 75 to 840 pM, corresponding to 5–63 ng mL⁻¹ enzyme equivalent (Table 2; ESM Fig. S3). Other groups reported LLOQs in a similar range for MRM³-based quantification on comparable instruments; e.g., several proteins were quantified down to concentrations between 10 and 80 ng mL⁻¹ in human serum [35], the LLOQs of two inflammation markers were 7.8 and 156 ng mL⁻¹ in plasma [38], and aquaporin-2 water channel protein could be measured at levels down to 0.5 ng mL⁻¹ in human urine (corresponding to 5 ng mL⁻¹ in the measuring solution) [36]. Here, the LLOQs were two up to tenfold lower in comparison to MRM-based quantification in matrix [35, 36, 38]. MS³ leads to lower signal intensities than MRM due to inevitable losses during each fragmentation step. Thus, the sensitivity gain of

MRM³ strongly depends on the reduction of interfering signals in biological matrices — the increased selectivity compensates the signal intensity loss [39]. The MRM detection of standards was up to tenfold more sensitive compared to MRM³ (Table 1, 2; ESM Fig. S3) and provided sufficient sensitivity and selectivity in cell matrix. However, the additional MS³ filtering stage proved helpful to separate the COX-2 peptide FDPPELLFNK from closely eluting background matrix in THP-1 cells (Fig. 2B (i), (ii)).

A relevant parameter for quantitative analysis is the number of data points per peak which is defined by the instrument cycle time. In order to enable MRM³, the MS method was subdivided into ten time periods (Fig. 2A (i); Table 2) in order to keep these within an accepted range of 10–15 data points per peak (FWHM). Summing the excitation time (25 ms for each MS³ fragmentation), FFT (250/100 and 25 ms), and individual scan times per peptide (scan ranges 450–700 Da), the cycle times per period in the MRM³ method were all below 600 ms, thus, allowing the detection of acceptable 9–12 data points per peak (FWHM). The long cycle times of the LIT have already been addressed as drawback of MRM³ methodology drastically limiting the number of concurrently measurable analytes [39, 40] and thus multiplexing capacities. This might be one of the reasons why MRM³ has not (yet) been employed for the analysis of (highly) multiplexed methods, e.g., the targeted analysis of pathway proteomes.

In our view, due to these drawbacks, (i) limited linear range, (ii) higher LLOQs, and (iii) limited multiplexing capacities based on the long cycle times and the use of time periods, the MRM³ method is not favored for routine analysis of pathway proteomes such as the ARA cascade. However, it serves as complimentary method, in case of heavy matrix background interference disturbing MRM analysis.

Combining this targeted proteomics approach with our oxylipin metabolomics method, we comprehensively characterized the ARA cascade in immune cells for the first time solely by LC–MS/MS in a single sample. This is especially advantageous for experiments with limited biological material such as primary human cells or tissue also known as single-platform multi-omics [41]. Moreover, if applicable, further merging the sample preparation techniques of proteomics and metabolomics also reduces sample preparation time [42].

The analysis of monocytic THP-1 cells showed that differentiation with VD₃ and TGFβ1 to macrophage-like cells led to the induction of *ALOX5* gene expression together with a drastic increase in levels of oxylipins (Fig. 3A (i), (ii)). VD₃/TGFβ1-based differentiation and concomitant increase of *ALOX5* gene activity have been described for several myeloid cell lines (HL-60, Mono Mac 6, THP-1) [43–46]. Concomitant upregulation of the FLAP protein or mRNA levels (Fig. 3A (ii)) were also reported during similar

treatments in peripheral blood monocytic cells [47] or the monocytic cell line U937 [48].

The LPS treatment induced upregulation of COX-2 abundance together with increased product formation (Fig. 3A (i)–(iii)). With the quantitative multi-omics approach, we could show a dose-dependent inhibition of LPS-induced PGE₂ formation and *PTGS2* gene expression by dexamethasone for the first time. Both determined IC₅₀ were similar (IC₅₀ = 1.2 nM and 3.4 nM) (Fig. 3A (iv)). This is consistent with the described mechanism of dexamethasone i.a. preventing the *PTGS2* gene expression by its mRNA destabilization [49] and concomitantly reducing PGE₂ formation. The remarkable potencies of dexamethasone in THP-1 macrophages were well within the range determined for inhibited PGE₂ formation (IC₅₀ = 1.6 nM; 95% CI, 1.4–1.9 nM) in LPS-stimulated human monocytes [50]. No IC₅₀ values have been determined for the inhibition of the *PTGS2* gene expression with the commonly used semi-quantitative western blot method (relevant inhibition detected at 3 nM to 1 μM) [50, 51]; thus, the novel targeted proteomics method offers new opportunities for such detailed characterization. The competitive 5-LOX inhibitor PF4191834 strongly inhibited 5-LOX product formation in differentiated and LPS-treated THP-1 cells without affecting the 5-LOX abundance (IC₅₀ (5-HETE) = 26 nM) (Fig. 3A (v)) fivefold more potently than in human whole blood assay (IC₅₀ (LTB₄) = 130 ± 10 nM) [52]. The commonly used iron–ligand inhibitor zileuton as well as the FLAP inhibitor MK886 had only low inhibitory potential in this cell model which might be caused by interferences induced by the VD₃/TGFβ1 and/or LPS treatment.

The multi-omics approach allows to obtain true *quantitative* information on the oxylipin concentrations and enzyme abundance levels with sensitive LC–MS/MS methods. For the first time, differently polarized primary human macrophages were characterized with this unique approach and displayed distinct oxylipin and protein patterns for each type (Fig. 3B (i), (ii)). In the non-CSF-treated macrophages (M0-like cells), only COX-1, 12-LOX, and its product 12-HETE were found. This pattern strongly resembles that of platelets (ESM Table S11) [53] which often contaminate monocyte preparations [54]. The presence of other enzymes (5-LOX, FLAP, and 15-LOX-2) and oxylipins at very low abundances as previously reported in M0-like macrophages [24] could not be supported. 5-LOX and FLAP were detected in M1- (CSF-2 and IFNγ-treated) and M2-like (CSF-1 and IL-4 treated) macrophages together with the corresponding oxylipins formed via this pathway (Fig. 3B (i), (ii); ESM Table S12). Varying 5-LOX levels between M1- and M2-like macrophages have been described [24, 55, 56] and thus might be donor-dependent. However, the relatively low 5-HETE concentrations in both macrophage types suggest only low 5-LOX activity and the detected

5-HETE levels could also result from autoxidation. Similarly, the data from the multi-omics investigation showing low levels of 12- and 15-HETE in M1-like macrophages could not be associated to LOX enzyme activity, since 12- and 15-LOX as well as 15-LOX-2 were below the detection limits and thus might be also formed autoxidatively (Fig. 3B (i), (ii), ESM Table S12). The correlation between the ten-fold increased 15-HETE concentration and LPS-stimulated COX-2 upregulation in our work is consistent with previous studies demonstrating that 15-HETE is a side product of COX(-2) [57, 58]. In the M2-like macrophages, the multi-omics approach showed that high 15-HETE concentrations dominated their lipid mediator profile which coincided with the presence of 15-LOX and 15-LOX-2 in these cells. This is expected because IL-4 is used during differentiation to M2-like macrophages, causing a strong elevation of 15-LOX and 15-LOX-2 abundances [24, 59, 60]. The dual reaction specificity of 15-LOX [61, 62] giving rise to both 15-HETE as well as 12-HETE also explains the formation of the second most abundant oxylipin 12-HETE in M2-like macrophages which was detected in parallel with the targeted oxylipin metabolomics method. Constitutive *PTGS1* gene expression and LPS-induced *PTGS2* expression were measured in both macrophage types. COX-2 abundances in both macrophage types were comparable, but LPS stimulation led to a more pronounced increase in product synthesis (PGE₂ and 12-HHT) in M1- vs. M2-like macrophages (Fig. 3B (i), (ii); ESM Table S12). Higher PGE₂ formation in M1-like cells is also in line with previous reports [24, 55].

The dual targeted oxylipin metabolomics and proteomics approach also allows the detailed investigation of quantitative changes induced by pharmaceuticals on both metabolite and enzyme levels of the ARA cascade (Fig. 4; ESM Table S13).

The COX inhibitors hampered the synthesis of PGE₂ and 12-HHT in M1- and M2-like macrophages. Indomethacin almost completely blocked product formation — inhibiting COX-1 and COX-2 [63] without affecting the enzyme abundance. Dexamethasone and celecoxib showed less inhibitory effects on product formation due to their specificity to only target COX-2 by direct specific inhibition in case of celecoxib [63] or reduction of its expression by the glucocorticoid dexamethasone [49]. The effect of the latter is also reflected in the results of the targeted proteomics analysis: markedly decreased COX-2 protein levels in M1- and M2-like macrophages (Fig. 4B). Interestingly, 15-HETE formation was reduced to a similar extent as the COX pathway products in indomethacin-like or dexamethasone-treated M1-like but not in the M2-like macrophages. This again demonstrated that 15-HETE must be predominately formed as COX product in M1-like macrophages as byproduct to prostaglandin synthesis [57, 58], while 15-HETE is mainly produced in M2-like macrophages by 15-LOX and 15-LOX-2. The

finding underlines that the complexity of the ARA cascade can only be addressed with the use of comprehensive methods such as our multi-omics approach. It also showed that the other prominent LOX pathway products were hardly affected by the COX inhibitors, and only celecoxib caused a notable shunt (increased formation) towards the formation of the hydroxy fatty acids (ESM Table S13). The 5-LOX inhibitor PF4191834 hardly inhibited the 5-HETE formation in M1-like macrophages without a substrate shunt towards the other enzymes (Fig. 4A; ESM Table S13) at a concentration 40-fold above the reported IC₅₀ in human whole blood [52]. These results from the multi-omics analysis thus indicate that 5-LOX is hardly active in M1-like macrophages and that 5-HETE seems to be predominantly formed by autoxidation. The determined oxylipin pattern in M2-like macrophages again highlighted the dual reaction specificity of the 15-LOX [61, 62] as its inhibitor ML351 reduced both 12- and 15-HETE concentrations to the same extent. It showed only minimal inhibitory activity towards the other ARA cascade enzymes as described by [64] and rather promoted a substrate shunt towards the COX products. The parallel analysis of the cells with the targeted proteomics method supported that the inhibitor acted only on enzyme activity as the 15-LOX level remained unchanged (Fig. 4; ESM Table S13).

With our comprehensive multi-omics approach, we showed clear correlations between the product and enzyme patterns in different human immune cells. Quantitative changes induced by different pharmaceuticals were assessed on both oxylipin and protein levels providing insights into their modes of action on the modulation of the ARA cascade.

Conclusion

The combination of the developed proteomics method with our targeted oxylipin metabolomics platform as multi-omics approach allows the quantitative investigation of 239 oxylipins and all COX (COX-1 and COX-2), relevant LOX pathway enzymes (5-, 12-, and 15-LOX, 15-LOX-2, and FLAP) from a single sample. MRM-based detection in proteomics is more favorable compared to MRM³ for investigation of the ARA cascade in immune cells due to its higher sensitivity, greater linear range, and higher multiplexing capacities. However, in case of matrix interference, MRM³ can be helpful. The application of the combined sensitive oxylipin metabolomics and proteomics approach to different human immune cells proved its usefulness in the thorough characterization of the ARA cascade. Here, it allowed the examination of quantitative changes induced by pharmaceuticals on oxylipin and enzyme abundance levels. Thus, this multi-omics strategy is an indispensable tool to study molecular modes of

action involved in the modulation of the ARA cascade and can be used in the future for the investigation, e.g., of novel pharmaceuticals or phytochemicals.

Supplementary Information The online version contains supplementary material available at <https://doi.org/10.1007/s00216-022-04489-3>.

Funding Open Access funding enabled and organized by Projekt DEAL. This work was supported by a Ph.D. fellowship from the Fonds der Chemischen Industrie to NMH and a grant (SCHE 1801) of the German Research Foundation (DFG) to NHS.

Declarations

Ethics approval Blood samples were drawn with the informed consent of the human subjects. The study was approved by the Ethical Committee of the University of Wuppertal.

Competing interests The authors declare no competing interests.

Open Access This article is licensed under a Creative Commons Attribution 4.0 International License, which permits use, sharing, adaptation, distribution and reproduction in any medium or format, as long as you give appropriate credit to the original author(s) and the source, provide a link to the Creative Commons licence, and indicate if changes were made. The images or other third party material in this article are included in the article's Creative Commons licence, unless indicated otherwise in a credit line to the material. If material is not included in the article's Creative Commons licence and your intended use is not permitted by statutory regulation or exceeds the permitted use, you will need to obtain permission directly from the copyright holder. To view a copy of this licence, visit <http://creativecommons.org/licenses/by/4.0/>.

References

- Gabbs M, Leng S, Devassy JG, Monirujjaman M, Aukema HM. Advances in our understanding of oxylipins derived from dietary PUFAs. *Adv Nutr*. 2015;6(5):513–40.
- Yu R, Xiao L, Zhao G, Christman JW, van Breemen RB. Competitive enzymatic interactions determine the relative amounts of prostaglandins E₂ and D₂. *J Pharmacol Exp Ther*. 2011;339(2):716–25.
- Matsunobu T, Okuno T, Yokoyama C, Yokomizo T. Thromboxane A synthase-independent production of 12-hydroxyheptadecatrienoic acid, a BLT2 ligand. *J Lipid Res*. 2013;54(11):2979–87.
- Ricciotti E, FitzGerald GA. Prostaglandins and inflammation. *Arterio Thromb Vasc Biol*. 2011;31(5):986–1000.
- Sheppe AEF, Edelmann MJ, Ottemann KM. Roles of eicosanoids in regulating inflammation and neutrophil migration as an innate host response to bacterial infections. *Infect Immun*. 2021;89(8):e00095–e121.
- Okuno T, Yokomizo T. Metabolism and biological functions of 12(S)-hydroxyheptadeca-5Z,8E,10E-trienoic acid. *Prostaglandins Other Lipid Mediat*. 2021;152:106502.
- Rund KM, Nolte F, Doricic J, Greite R, Schott S, Lichtinghagen R, et al. Clinical blood sampling for oxylipin analysis – effect of storage and pneumatic tube transport of blood on free and total oxylipin profile in human plasma and serum. *Analyst*. 2020;145(6):2378–88.
- Kuhn H, Banthiya S, van Leyen K. Mammalian lipoxygenases and their biological relevance. *Biochim Biophys Acta, Mol Cell Biol Lipids*. 2015;1851(4):308–30.
- Serhan CN, Chiang N, Van Dyke TE. Resolving inflammation: dual anti-inflammatory and pro-resolution lipid mediators. *Nat Rev Immunol*. 2008;8(5):349–61.
- Schebb NH, Kühn H, Kahnt AS, Rund KM, O'Donnell VB, Flament N, et al. Formation, signaling and occurrence of specialized pro-resolving lipid mediators—what is the evidence so far? *Front Pharmacol*. 2022;13:838782.
- Pinu FR, Beale DJ, Paten AM, Kouremenos K, Swarup S, Schirra HJ, et al. Systems biology and multi-omics integration: viewpoints from the metabolomics research community. *Metabolites*. 2019;9(4):76.
- Canzler S, Schor J, Busch W, Schubert K, Rolle-Kampczyk UE, Seitz H, et al. Prospects and challenges of multi-omics data integration in toxicology. *Arch Toxicol*. 2020;94(2):371–88.
- Gladine C, Ostermann AI, Newnham JW, Schebb NH. MS-based targeted metabolomics of eicosanoids and other oxylipins: analytical and inter-individual variabilities. *Free Radical Biol Med*. 2019;144:72–89.
- Hanáková Z, Hošek J, Kutil Z, Temml V, Landa P, Vaněk T, et al. Anti-inflammatory activity of natural geranylated flavonoids: cyclooxygenase and lipoxygenase inhibitory properties and proteomic analysis. *J Nat Prod*. 2017;80(4):999–1006.
- Rodríguez-Blanco G, Zenayedpour L, Duijvesz D, Hoogland AM, Verhoeve EI, Kweldam CF, et al. Tissue proteomics outlines AGR2 AND LOX5 as markers for biochemical recurrence of prostate cancer. *Oncotarget*. 2018;9(92):36444–56.
- Codreanu SG, Hoeksema MD, Slebos RJC, Zimmerman LJ, Rahman SMJ, Li M, et al. Identification of proteomic features to distinguish benign pulmonary nodules from lung adenocarcinoma. *J Proteome Res*. 2017;16(9):3266–76.
- Jethwaney D, Islam MR, Leidal KG, de Bernabe DBV, Campbell KP, Nauseef WM, et al. Proteomic analysis of plasma membrane and secretory vesicles from human neutrophils. *Proteome Sci*. 2007;5(1):12.
- Hartung NM, Ostermann AI, Immenschuh S, Schebb NH. Combined targeted proteomics and oxylipin metabolomics for monitoring of the COX-2 pathway. *Proteomics*. 2021;21(3–4):1900058.
- Sabido E, Quehenberger O, Shen Q, Chang CY, Shah I, Armando AM, et al. Targeted proteomics of the eicosanoid biosynthetic pathway completes an integrated genomics-proteomics-metabolomics picture of cellular metabolism. *Mol Cell Proteomics*. 2012;11(7):M111.014746.
- Tahir A, Bileck A, Muqaku B, Niederstaetter L, Kreutz D, Mayer RL, et al. Combined proteome and eicosanoid profiling approach for revealing implications of human fibroblasts in chronic inflammation. *Anal Chem*. 2017;89(3):1945–54.
- Rund KM, Ostermann AI, Kutzner L, Galano JM, Oger C, Vigor C, et al. Development of an LC-ESI(-)MS/MS method for the simultaneous quantification of 35 isoprostanes and isofurans derived from the major n3- and n6-PUFAs. *Anal Chim Acta*. 2018;1037:63–74.
- Kutzner L, Rund KM, Ostermann AI, Hartung NM, Galano JM, Balas L, et al. Development of an optimized lc-ms method for the detection of specialized pro-resolving mediators in biological samples. *Front Pharmacol*. 2019;10:169.
- Koch E, Mainka M, Dalle C, Ostermann AI, Rund KM, Kutzner L, et al. Stability of oxylipins during plasma generation and long-term storage. *Talanta*. 2020;217:121074.
- Ebert R, Cumbana R, Lehmann C, Kutzner L, Toewe A, Ferreira N, et al. Long-term stimulation of toll-like receptor-2 and -4 upregulates 5-LO and 15-LO-2 expression thereby inducing a lipid mediator shift in human monocyte-derived macrophages. *Biochim Biophys Acta, Mol Cell Biol Lipids*. 2020;1865(9):158702.
- Dhurat R, Sukesh M. Principles and methods of preparation of platelet-rich plasma: a review and author's perspective. *J Cutan Aesthet Surg*. 2014;7(4):189–97.

26. O'Brien J, Wilson I, Orton T, Pognan F. Investigation of the Alamar Blue (resazurin) fluorescent dye for the assessment of mammalian cell cytotoxicity. *Eur J Biochem.* 2000;267(17):5421–6.
27. Smith PK, Krohn RI, Hermanson GT, Mallia AK, Gartner FH, Provenzano MD, et al. Measurement of protein using bicinchoninic acid. *Anal Biochem.* 1985;150(1):76–85.
28. Johnson M, Zaretskaya I, Raytselis Y, Merezuk Y, McGinnis S, Madden TL. NCBI BLAST: a better web interface. *Nucleic Acids Res.* 2008;36(suppl_2):W5–9.
29. Schaeffer M, Gateau A, Teixeira D, Michel PA, Zahn-Zabal M, Lane L. The neXtProt peptide uniqueness checker: a tool for the proteomics community. *Bioinformatics.* 2017;33(21):3471–2.
30. Gasteiger E, Hoogland C, Gattiker A, Duvaud S, Wilkins MR, Appel RD, et al. Protein identification and analysis tools on the ExPASy server. In: Walker JM, editor., et al., *The Proteomics Protocols Handbook*. Totowa: Humana Press; 2005. p. 571–607.
31. Fannes T, Vandermarliere E, Schietgat L, Degroove S, Martens L, Ramon J. Predicting tryptic cleavage from proteomics data using decision tree ensembles. *J Proteome Res.* 2013;12(5):2253–9.
32. Krokikh OV, Spicer V. Peptide retention standards and hydrophobicity indexes in reversed-phase high-performance liquid chromatography of peptides. *Anal Chem.* 2009;81(22):9522–30.
33. The Uniprot Consortium. UniProt: a worldwide hub of protein knowledge. *Nucleic Acids Res.* 2018;47(D1):D506–15.
34. Hornbeck PV, Zhang B, Murray B, Kornhauser JM, Latham V, Skrzypek E. PhosphoSitePlus, 2014: mutations, PTMs and recalibrations. *Nucleic Acids Res.* 2015;43(D1):D512–20.
35. Fortin T, Salvador A, Charrier JP, Lenz C, Bettsworth F, Lacoux X, et al. Multiple reaction monitoring cubed for protein quantification at the low nanogram/milliliter level in nondepleted human serum. *Anal Chem.* 2009;81(22):9343–52.
36. Jaffuel A, Lemoine J, Aubert C, Simon R, Léonard J-F, Gautier J-C, et al. Optimization of liquid chromatography–multiple reaction monitoring cubed mass spectrometry assay for protein quantification: application to aquaporin-2 water channel in human urine. *J Chromatogr.* 2013;1301:122–30.
37. Korte R, Brockmeyer J. MRM3-based LC-MS multi-method for the detection and quantification of nut allergens. *Anal Bioanal Chem.* 2016;408(27):7845–55.
38. Jeudy J, Salvador A, Simon R, Jaffuel A, Fonbonne C, Léonard J-F, et al. Overcoming biofluid protein complexity during targeted mass spectrometry detection and quantification of protein biomarkers by MRM cubed (MRM3). *Anal Bioanal Chem.* 2014;406(4):1193–200.
39. Lemoine J, Fortin T, Salvador A, Jaffuel A, Charrier J-P, Choquet-Kastylevsky G. The current status of clinical proteomics and the use of MRM and MRM3 for biomarker validation. *Expert Rev Mol Diagn.* 2012;12(4):333–42.
40. Schmidlin T, Garrigues L, Lane CS, Mulder TC, van Doorn S, Post H, et al. Assessment of SRM, MRM3, and DIA for the targeted analysis of phosphorylation dynamics in non-small cell lung cancer. *Proteomics.* 2016;16(15–16):2193–205.
41. Blum BC, Mousavi F, Emili A. Single-platform 'multi-omic' profiling: unified mass spectrometry and computational workflows for integrative proteomics–metabolomics analysis. *Mol Omics.* 2018;14(5):307–19.
42. Zougman A, Wilson JP, Roberts LD, Banks RE. Detergent-free simultaneous sample preparation method for proteomics and metabolomics. *J Proteome Res.* 2020;19(7):2838–44.
43. Brungs M, Radmark O, Samuelsson B, Steinhilber D. On the induction of 5-lipoxygenase expression and activity in HL-60 Cells: effects of vitamin D3, retinoic acid, DMSO and TGF β . *Biochem Biophys Res Commun.* 1994;205(3):1572–80.
44. Brungs M, Radmark O, Samuelsson B, Steinhilber D. Sequential induction of 5-lipoxygenase gene-expression and activity in mono-Mac-6 cells by transforming growth-factor-beta and 1,25-dihydroxyvitamin-D3. *Proc Natl Acad Sci U S A.* 1995;92(1):107–11.
45. Wöbke TK, von Knethen A, Steinhilber D, Sorg BL. CD69 is a TGF- β /1 α ,25-dihydroxyvitamin D3 target gene in monocytes. *PLoS ONE.* 2013;8(5):e64635.
46. Schlag K, Steinhilber D, Karas M, Sorg BL. Analysis of proximal ALOX5 promoter binding proteins by quantitative proteomics. *FEBS J.* 2020;287(20):4481–99.
47. Coffey MJ, Gyetko M, Peters-Golden M. 1,25-Dihydroxyvitamin D3 upregulates 5-lipoxygenase metabolism and 5-lipoxygenase activating protein in peripheral blood monocytes as they differentiate into mature macrophages. *J Lipid Mediators.* 1993;6(1–3):43–51.
48. Gingras M-C, Margolin JF. Differential expression of multiple unexpected genes during U937 cell and macrophage differentiation detected by suppressive subtractive hybridization. *Exp Hematol.* 2000;28(1):65–76.
49. Lasa M, Brook M, Saklatvala J, Clark AR. Dexamethasone destabilizes cyclooxygenase 2 mRNA by inhibiting mitogen-activated protein kinase p38. *Mol Cell Biol.* 2001;21(3):771–80.
50. Willenberg I, Meschede AK, Schebb NH. Determining cyclooxygenase-2 activity in three different test systems utilizing online-solid phase extraction-liquid chromatography-mass spectrometry for parallel quantification of prostaglandin E(2), D(2) and thromboxane B(2). *J Chromatogr A.* 2015;1391:40–8.
51. Laufer S, Zechmeister P, Klein T. Development of an in-vitro test system for the evaluation of cyclooxygenase-2 inhibitors. *Inflammation Res.* 1999;48(3):133–8.
52. Masferrer JL, Zweifel BS, Hardy M, Anderson GD, Dufield D, Cortes-Burgos L, et al. Pharmacology of PF-4191834, a novel, selective non-redox 5-lipoxygenase inhibitor effective in inflammation and pain. *J Pharmacol Exp Ther.* 2010;334(1):294.
53. O'Donnell VB, Murphy RC, Watson SP. Platelet lipidomics. *Circul Res.* 2014;114(7):1185–203.
54. Prokopi M, Pula G, Mayr U, Devue C, Gallagher J, Xiao Q, et al. Proteomic analysis reveals presence of platelet micro-particles in endothelial progenitor cell cultures. *Blood.* 2009;114(3):723–32.
55. Werner M, Jordan PM, Romp E, Czupka A, Rao Z, Kretzer C, et al. Targeting biosynthetic networks of the proinflammatory and proresolving lipid metabolome. *FASEB J.* 2019;33(5):6140–53.
56. Werz O, Gerstmeier J, Libreros S, De la Rosa X, Werner M, Norris PC, et al. Human macrophages differentially produce specific resolvins or leukotriene signals that depend on bacterial pathogenicity. *Nat Comm.* 2018;9(1):59.
57. Hecker M, Ullrich V, Fischer C, Meese CO. Identification of novel arachidonic acid metabolites formed by prostaglandin H synthase. *Eur J Biochem.* 1987;169(1):113–23.
58. O'Neill GP, Mancini JA, Kargman S, Yergey J, Kwan MY, Falgout JP, et al. Overexpression of human prostaglandin G/H synthase-1 and -2 by recombinant vaccinia virus: inhibition by nonsteroidal anti-inflammatory drugs and biosynthesis of 15-hydroxyicosatetraenoic acid. *Mol Pharmacol.* 1994;45(2):245–54.
59. Wuest SJA, Crucet M, Gemperle C, Loretz C, Hersberger M. Expression and regulation of 12/15-lipoxygenases in human primary macrophages. *Atherosclerosis.* 2012;225(1):121–7.
60. Snodgrass RG, Zezina E, Namgaladze D, Gupta S, Angioni C, Geisslinger G, et al. A novel function for 15-lipoxygenases in cholesterol homeostasis and CCL17 production in human macrophages. *Front Immunol.* 2018;9:1906.
61. Kühn H, Barnett J, Grunberger D, Baecker P, Chow J, Nguyen B, et al. Overexpression, purification and characterization of human recombinant 15-lipoxygenase. *Biochim Biophys Acta, Lipids Lipid Metab.* 1993;1169(1):80–9.

62. Kutzner L, Goloshchapova K, Heydeck D, Stehling S, Kuhn H, Schebb NH. Mammalian ALOX15 orthologs exhibit pronounced dual positional specificity with docosahexaenoic acid. *Biochim Biophys Acta, Mol Cell Biol Lipids*. 2017;1862(7):666–75.
63. Willenberg I, Meschede AK, Gueller F, Jang MS, Shushakova N, Schebb NH. Food polyphenols fail to cause a biologically relevant reduction of COX-2 activity. *PLoS ONE*. 2015;10(10):e0139147.
64. Rai G, Joshi N, Jung JE, Liu Y, Schultz L, Yasgar A, et al. Potent and selective inhibitors of human reticulocyte 12/15-lipoxygenase as anti-stroke therapies. *J Med Chem*. 2014;57(10):4035–48.

Publisher's Note Springer Nature remains neutral with regard to jurisdictional claims in published maps and institutional affiliations.